Exp Oncol 2012
34, 3, 269–276

INVITED REVIEW

Experimental ONCOLOGY

ANTICANCER THERAPY AND APOPTOSIS IMAGING

T.J. Yang[1], A. Haimovitz-Friedman[1], M. Verheij[2,]*

[1]Department of Radiation Oncology, Memorial Sloan-Kettering Cancer Center, New York 10065, USA

[2]Department of Radiation Oncology and Division of Biological Stress Response, The Netherlands Cancer Institute – Antoni van Leeuwenhoek Hospital, 1066 CX, Amsterdam, The Netherlands

Early response prediction is considered an essential tool to obtain a more customized anticancer treatment because it allows for the identification of patients who will benefit most from a particular therapy and prevents the exposure of those patients to toxic, non-effective regimens. Recent discoveries of novel markers in functional imaging have created exciting opportunities for *in vivo* visualization and quantification of cell death. This review will focus on *in vivo* apoptosis imaging with various radiotracers as predictive tools for tumor response after anticancer therapy. Particular focus will be on annexin V imaging, a technique with the largest clinical experience to date. This article is part of a Special Issue entitled "Apoptosis: Four Decades Later".

***Key Words*: apoptosis, cell death, imaging, anticancer therapy, annexin V.**

INTRODUCTION

Apoptosis is an evolutionary highly preserved and well-orchestrated biological process involved in both physiological and pathological conditions, and therefore possibly the most abundant form of programmed cell death [1]. Therapy-induced apoptosis *in vivo* has been shown to significantly contribute to tumor response [2, 3] and to correlate with subsequent outcome [4–6]. After 40 years of intense research, apoptosis is now considered not only as a fundamental process leading to disorders of normal tissues [7–10], but also as a form of cell death in response to oncolytic therapies [11–14].

Apoptosis can be triggered by exogenous and endogenous stimuli leading to the activation of the extrinsic and intrinsic pathways of apoptosis, respectively (Fig. 1). These pathways converge at the activation of a subset of proteases, the executioner caspase-3, -6 and -7, targeting specific intracellular proteins such as those involved in DNA damage repair and cellular cytoskeleton.

Received: June 25, 2012

*Correspondence: Phone: +31 20 512-21-20
Fax: +31 20 669-11-01
E-mail: m.verheij@nki.nl

Abbreviations used: ^{99m}Tc – ^{99m}Technetium; Apaf-1 – apoptotic activating factor-1; BTAP – 4,5-bis(thioacetamido)pentanoyl; CT – computed tomography; DD – death domain; DED – death effector domain; DISC – death-inducing signaling complex; DR – death receptor; FADD – Fas-associated death domain; FasL – Fas ligand; HL – Hodgkin lymphoma; HNSCC – head and neck squamous cell carcinoma; HYNIC – hydrazinonicotinamide; MDR1 – multidrug resistance gene 1; MIBI – methoxyisobutylisonitrile; NHL – non-Hodgkin lymphoma; NSCLC – non-small cell lung cancer; PARA – pro-apoptotic receptor agonist; PARP-1 – poly-ADP-ribose polymerase 1; PET – positron emission tomography; PS – phosphatidylserine; SCLC – small cell lung cancer; SPECT – single photon emission computerized tomography; TAVS – ^{99m}Tc-annexin V scintigraphy; TNF-α – tumor necrosis factor α; TNFR1 – TNF receptor 1; TRADD – TNF-receptor-associated death domain; TRAIL – TNF-related apoptosis-inducing ligand; TUNEL – terminal deoxynucleotidyl transferase-mediated dUTP–biotin nick end labeling.

The extrinsic pathway is engaged by binding of specific death ligands to specific death receptors on the cell membrane, such as tumor necrosis factor α (TNF-α), TNF-related apoptosis-inducing ligand (TRAIL), Fas ligand (FasL) to TNF receptor 1 (TNFR1), death receptor 4 or death receptor 5 (DR4 or DR5) and Fas/CD95 receptor, respectively. Death receptor-ligand binding recruits an intracellular adaptor molecule, TNF-receptor-associated death domain (TRADD) or Fas-associated death domain (FADD) via its cytoplasmic death domain (DD), clustering to form the death-inducing signaling complex (DISC) which in turn recruits and activates cytoplasmic pro-apoptotic caspase-8 (initiator caspase) via its death effector domain (DED). This is followed by the sequential activation of downstream executioner caspase-3, -6, and -7. Activated caspase-3 translocates to the nucleus and activates poly-ADP-ribose polymerase (PARP-1), which facilitates the degradation of nuclear DNA into 50 to 300 kilobase-sized fragments.

Anticancer drugs and ionizing radiation utilize the intrinsic pathway to trigger apoptosis. This process involves mitochondrial outer membrane permeabilization and the subsequent release of pro-apoptotic factors, including cytochrome *c*, into the cytosol. Cytochrome *c* interacts with Apaf-1 (apoptotic activating factor-1), ATP, and procaspase-9 to form a complex known as the apoptosome which in turn activates caspase-9 and further activates the executioner caspase-3, -6, and -7, generating a variety of molecular damages in essentially every organelle. In terms of cell survival, however, it is the damage to DNA leading to the loss of proliferative and clonogenic capacity that is most important. Although chemotherapy and radiotherapy-induced apoptosis is a caspase-dependent process [15–18], it is unclear how cellular signals from DNA lesions lead to the execution of apoptosis. Since Bcl-2 is able to block cytochrome *c* release and prevent apoptosis, it has been proposed that anticancer therapy-induced caspase activation is mitochondria dependent [17, 19–21]. This concept

is further substantiated by the observation that activation of p53 by anticancer therapy due to DNA damage is a direct transcriptional regulator of Bcl-2, Bax, Puma, Noxa and Bid and can act as an apoptogenic factor at the mitochondrial membrane [22–25]. Furthermore, there are functional connections between p53 and death receptors genes (CD95 and TRAIL receptor-2) that can be upregulated in response to therapy [26, 27], in turn leading to the activation of inducer caspase-8. It has also been shown that pretreatment of cells with DNA damaging agents improves the capacity of TRAIL-bound receptors to recruit FADD and activate caspase-8 and -10 in the DISC, irrespective of p53 status [28].

As apoptosis has been recognized as a major form of cell death after anticancer therapy, it is being increasingly evaluated as a prognostic marker of treatment outcome. For this purpose, a noninvasive method to analyze treatment-induced apoptosis is most attractive, as it can be used to determine and predict the effectiveness of an anticancer regime. In this review, we will discuss apoptosis imaging modalities in both animal models and patients using annexin V, detection of apoptotic membrane imprint, methoxyisobutylisonitrile (MIBI), and the novel caspase-3 small-molecule inhibitor, Isatin, and address their ability to improve patient treatment (see Fig. 1). Annexin V scintigraphy, an imaging technique for which we have the most clinical experience with, will especially be detailed in this discussion.

IMAGING OF APOPTOSIS USING ANNEXIN V

Annexin V-based tracers are the most frequently used agents for *in vitro* detection and quantification of apoptotic cells. This is based on the high affinity of annexin V for the membrane bound phospholipid (PS), which in viable cells, resides in the inner leaflet of the plasma membrane. Upon exposure of cells to apoptotic stimuli γ-scramblase is activated resulting in PS flipping to the outer leaflet of the plasma membrane, thereby allowing annexin V to bind to PS. In addition, it has been shown that membrane binding of proteins that recognize exposed PS on apoptotic cells is regulated by the transmembrane potential [29]. A decreasing membrane potential in Jurkat T leukemia cells and K562 promyelocytic leukemia cells undergoing apoptosis increases the extracellular binding of annexin V in a dose-dependent manner. Studies with PS vesicles also showed that the membrane potential increases the binding affinity of annexin V for the PS cell surface molecules.

Single photon emission computed tomography (SPECT)

^{99m}Technetium-linked annexin V has been extensively used in apoptosis detection in patients, exploiting its optimal radionuclidic properties for SPECT

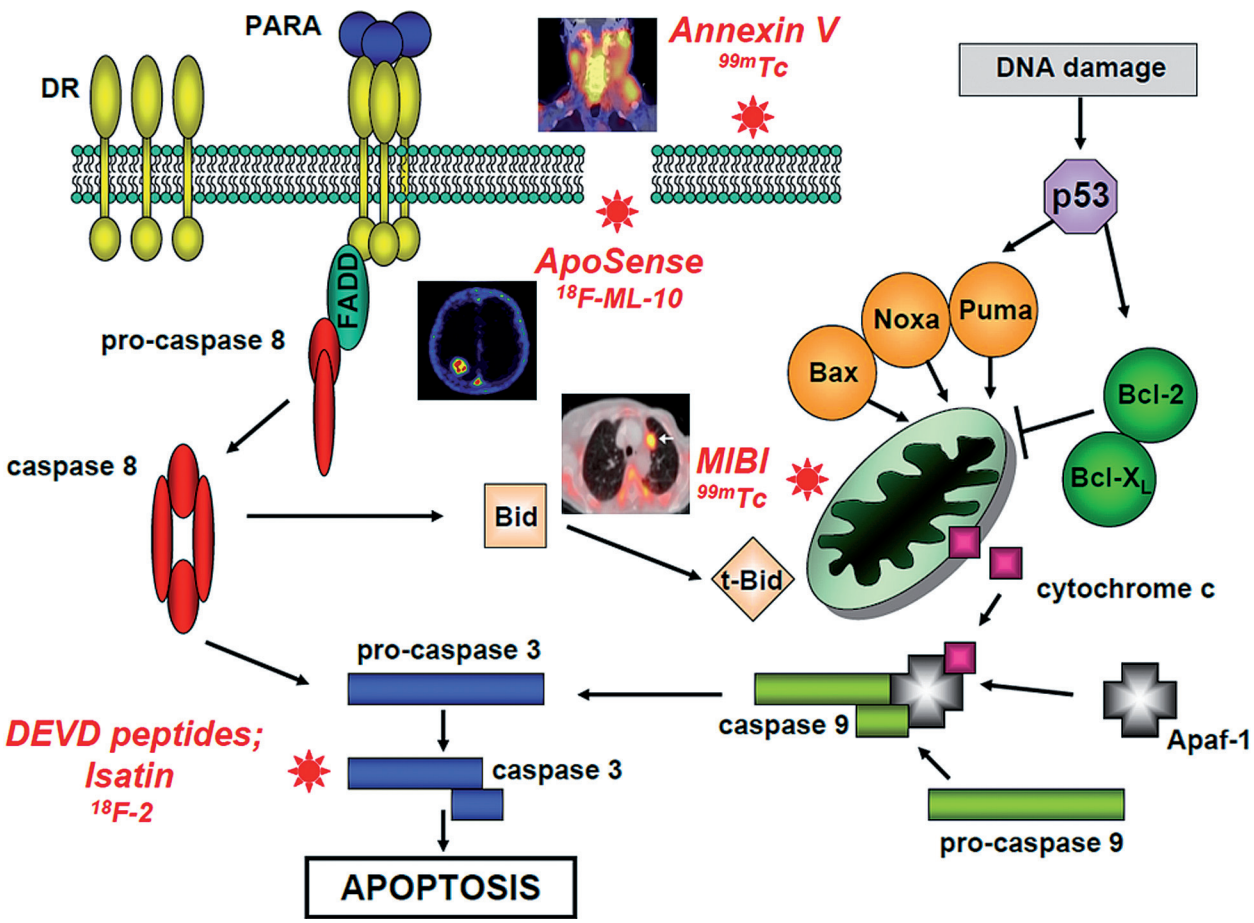

Fig. 1. Imaging of apoptosis by various radiotracers. While annexin V based compounds and ApoSense agents work at the level of the cell plasma membrane, MIBI acts at the mitochondria and Isatin targets executioner caspase 3 (DR=Death Receptor; PARA=Pro-Apoptotic Receptor Agonist). Inserts are examples of images acquired by the indicated modalities. Modified from: Haimovitz-Friedman et al., 2012 [94]

imaging, relative low costs and easy availability [30]. In 1995, Stratton *et al*. [31] were the first to demonstrate ^{99m}Tc-annexin V's value for the *in vivo* detection of membrane-associated PS exposure using SPECT by injecting ^{99m}Tc-labeled human annexin V intravenously and calculating the atrial thrombus/blood ratio in thrombo-embolic diseases. Other SPECT studies using ^{99m}Tc-annexin V derivatives provided feasibility and potential clinical utility of apoptosis imaging in various other medical disorders [32]. Multiple conjugators of annexin V have been developed, including 4,5-bis(thioacetamido)pentanoyl (BTAP) for its rapid and extensive radioactivity accumulation in the gastrointestinal tract. Since this tracer was mainly excreted by the liver and the kidneys, resulting in an increased radionuclide accumulation in these organs as well [33], the role of ^{99m}Tc-BTAP annexin V for abdominal imaging was limited.

Blankenberg *et al*. [34] subsequently coupled annexin V to hydrazinonicotinamide and created ^{99m}Tc-HYNIC annexin V. *In vivo* studies using a CD95L-induced hepatocyte apoptosis mouse model with intravenously administered anti-CD95 antibody demonstrated that ^{99m}Tc-HYNIC annexin V can be used to image apoptotic (and necrotic) cell death *in vivo*. Although the concentration of tracer in liver and kidneys were still high, and similar to ^{99m}Tc-BTAP annexin V, radioactivity accumulation in the bowel was eradicated, making it a suitable candidate tracer for abdominal examination [35]. Following further optimization of image quality, ^{99m}Tc-annexin V proves to be an effective modality for non-invasive evaluation of cell death and treatment response in allograft rejection, myocardial infarction, reperfusion injury and infectious disease [36–38].

^{99m}Tc-annexin V studies in combination with anticancer therapy

The first *in vivo* demonstration of anticancer therapy-induced apoptosis involved the use of ^{99m}Tc-annexin V in an experimental mouse lymphoma model treated with cyclophosphamide. The animals treated with chemotherapy demonstrated a more than 300% increase in annexin V uptake 20 h after treatment compared to untreated animals [39]. More recently, the value of ^{99m}Tc-annexin V imaging in response monitoring was evaluated in a mouse model for hereditary breast cancer after docetaxel treatment [40]. The sensitive tumors showed an increase in ^{99m}Tc-annexin V uptake and immunohistochemical evidence of apoptosis one day post-treatment. On the other hand, resistant tumors showed neither an increase in ^{99m}Tc-annexin V uptake nor significant immunohistochemical changes (Fig. 2). Despite these encouraging findings, ^{99m}Tc-annexin V imaging could not be used to predict tumor response, due to large variations in uptake between animals.

In addition to animal studies, annexin V imaging has also been applied in various clinical protocols. In 2002, ^{99m}Tc-annexin V was first used in clinical trials with patients scheduled to receive chemotherapy for locally advanced or metastatic non-small cell lung cancer (NSCLC), small cell lung cancer (SCLC), Hodgkin (HL) and non-Hodgkin (NHL) lymphoma, and breast cancer. Fifteen patients underwent ^{99m}Tc-annexin V scintigraphy before and within 3 days after their first course of chemotherapy. Patients with lung cancer received platinum-based chemotherapy, lymphoma patients were treated with vincristine or cyclophosphamide-based chemotherapy and breast cancer patients received taxane as their chemotherapy regime. Five patients had increased annexin V uptake 40–48 hours after chemotherapy (1 NHL, 1 HL, 1 SCLC, and 1 NSCLC), and 2 patients showed increased uptake 20–24 hours after treatment (1 NSCLC, 1 SCLC). At the median follow-up of 117 days, while patients with no change in radiotracer uptake after the first cycle of chemotherapy had no subsequent objective clinical response, patients demonstrating increased tracer uptake post-treatment had either a partial or complete tumor response. From these results, it was concluded that ^{99m}Tc-annexin V could be used clinically for *in vivo* imaging of apoptosis after one course of chemotherapy [41].

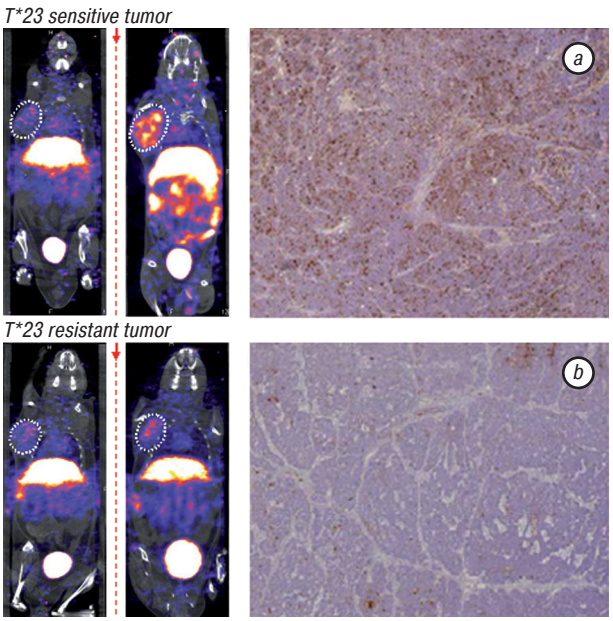

Fig. 2. Preclinical imaging of apoptosis. Quantitative whole animal ^{99m}Tc-annexin V SPECT imaging and histology of a T*23 sensitive (*a*) and resistant tumor (*b*), obtained before and 1 day after docetaxel treatment. Right panel: tumors were stained for TUNEL at day 1. Modified from: Beekman *et al*., 2011 [40]

One of the first reports on the application of ^{99m}Tc-annexin V in patients receiving radiotherapy was by Haas *et al*. [42] who applied ^{99m}Tc-annexin V scintigraphy (TAVS) to monitor radiation-induced apoptotic cell death in 11 follicular lymphoma patients (Fig. 3). All patients underwent a baseline scan within one week prior to the start of radiotherapy to detect baseline levels of spontaneous tumor apoptosis or necrosis. Patients were then irradiated to the involved lymph node areas to a total dose of 4 Gy in 2 fractions 48 h apart. At 24 h after the second radiation fraction, TAVS was repeated. Fine needle aspiration cytologic analysis for apoptosis was also performed prior to, during and after irradiation. In 10 patients, post-treatment TAVS

matched the post-treatment cytology, confirming TAVS as a valuable non-invasive method to detect *in vivo* apoptosis caused by radiation. In addition, the increase in ^{99m}Tc-annexin V uptake post-treatment in this type of malignancy correlated with clinical outcome: all patients with prominent cytologic and scintigraphic signs of apoptosis achieved complete remission within 1 week.

In 2004, Kartachova *et al*. [43] from the Netherlands Cancer Institute conducted a study of 33 patients with malignant lymphoma, leukemia, NSCLC, and head and neck squamous cell carcinoma (HNSCC) scheduled for radiotherapy, platinum-based chemotherapy, or concurrent chemoradiation (see Fig. 3).

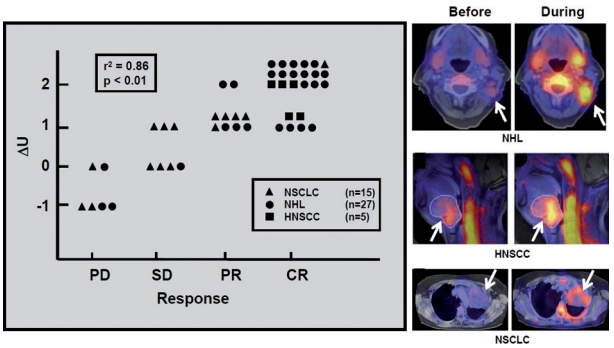

Fig. 3. Typical examples of anticancer therapy-induced apoptosis as demonstrated by *in vivo* annexin V scintigraphy. Shown are 3 examples of SPECT before (left panel) and early during treatment (i.e. 24–48 h after start of therapy; right panel). Upper panel: NHL treated by low dose (2x2 Gy) involved-field radiation. Middle panel: HNSCC treated by cisplatin-based chemoradiation. Lower panel: NSCLC treated by cisplatin/gemcitabine chemotherapy. Arrows indicate the target lesions. Note the physiologic uptake in bones and salivary glands (Modified from: Haas *et al*., 2004 [42] and Kartachova *et al*., 2004 [43], Kartachova *et al*., 2007 [44], and Verheij *et al*., 2008 [93]

The investigators demonstrated increased ^{99m}Tc-annexin V accumulation in lesions early during treatment when compared to baseline values in patients with complete or partial tumor remission, while there was no significant early increase in uptake in those patients with stable or progressive disease. This study established ^{99m}Tc-annexin V scintigraphy as a predictive marker in tumor response. A subsequent study from these authors evaluated the predictive value of TAVS in 16 chemotherapy-naive patients with advanced stage NSCLC undergoing platinum-based chemotherapy. Also under these conditions, a significant correlation between annexin V changes and treatment outcome was found [44]. In a 2008 update of their study, Kartachova *et al*. [45] showed that visual evaluation of SPECT images, SPECT/SPECT and SPECT/CT co-registered images correlated with quantitative analysis. Using both methods, all patients with early post-treatment increase in tumor uptake of ^{99m}Tc-annexin V either developed complete response or partial response, resulting in statistically highly significant correlations between changes of ^{99m}Tc-annexin V tumor uptake and therapeutic outcome for both visual and quantitative analysis.

In addition to the monitoring of treatment-induced apoptosis in tumor cells, TAVS may also be used to detect normal tissue toxicity. Hoebers *et al*. [46] applied ^{99m}Tc-annexin V scintigraphy to demonstrate apoptosis in patients with HNSCC, both in tumor and normal tissue. TAVS was performed before and within 48 h after the first course of cisplatin-based chemoradiation in 13 patients. Already after a dose of 6–8 Gy increased annexin V uptake was observed in 24 of the 26 irradiated parotid glands. Glands, which received higher radiation dosages, showed more annexin V uptake. The authors concluded that within the dose range of 0–8 Gy, TAVS showed a radiation-dose-dependent uptake in parotid glands, indicative of radiation-induced apoptosis. A similar pattern in the submandibular glands was observed.

Limitations of annexin V imaging

Although TAVS appears very promising as an early predictor for tumor response to anticancer therapy, several limitations remain to firmly establish its value as an imaging biomarker of response. First of all, apoptosis is an acute event and contributes to early therapy-induced tumor shrinkage. Therefore, TAVS may be less suitable to predict long-term response to treatment [47–49]. To determine whether this type of early cell death predicts long-term treatment outcome parameters in patients, such as disease-free survival and overall survival, changes in TAVS uptake should be correlated with tumor response measurements after sufficiently long follow-up. Secondly, annexin V binding to PS does not discriminate between apoptotic and necrotic cell death as disrupted plasma membranes also make PS accessible at the inner leaflet of cells undergoing necrosis. Thirdly, in terms of biodistribution, annexin V has a relatively slow clearing rate from non-targeted tissues, therefore creating a low signal-to-noise ratio [50]. Fourthly, the optimal timing of apoptosis-imaging *in vivo* that yields most predictive information in terms of tumor response remains uncertain and should ideally be determined for each specific tumor type and treatment modality. Multiple TAVS measurements may be necessary to define this tumor- and/or therapy-specific optimal timing. Finally, apoptosis represents only one aspect of the complex biological response to therapy, and its relative contribution varies among different tumor entities. More studies are needed to demonstrate the applicability of TAVS, especially in (solid) tumors that are therapy-resistant. Combining TAVS with other anatomical and functional imaging modalities may be helpful in obtaining a more complete, and perhaps more solid biomarker.

OTHER RADIOTRACERS IN APOPTOSIS IMAGING

Detection of apoptotic membrane imprint

The apoptotic membrane imprint is a complex of cellular changes occurring in the plasma membrane early during the apoptotic process. These include irreversible loss of membrane potential, permanent acidification of the external plasma membrane leaflet and cytosol, and activation of γ-scramblase while preserving the

integrity of the plasma membrane. A set of novel small-molecule probes designated the Aposense compounds (Aposense Ltd., Petach-Tikva, Israel) have been developed to detect these apoptosis-related plasma membrane alterations (see Fig. 1 [51]). This family of small molecules (DDC, ML-10, ML-9, NST-732, and NST-739) have demonstrated activities in a number of tumor models in response to anticancer agents [52–54], however there is no clear mechanism of uptake of these compounds. The positron emission tomography (PET) tracer ^{18}F-ML-10 shows selective uptake by apoptotic cells in tumors following radio- and chemotherapy, correlating with breakdown of mitochondrial membrane potential, caspase activation and DNA degradation. As the signal is lost upon rupture of the plasma membrane, ^{18}F-ML-10 should be capable of discriminating apoptotic from necrotic cells [51].

Recently, the role of ^{18}F-ML-10 was evaluated in the early detection of response of brain metastases to whole brain irradiation (10x3 Gy). In this study 10 patients underwent an ^{18}F-ML-10 PET scan prior to treatment and a second scan after 9 or 10 fractions of radiation. MRI was performed 6–8 weeks after completion of treatment. In all 10 patients, both MRI and the ^{18}F-ML-10 PET scan detected all brain lesions. A highly significant correlation was found between early changes on the ^{18}F-ML-10 scan and later changes in tumor anatomical dimensions on MRI [55].

Methoxyisobutylisonitrile (MIBI)

Technetium-99m methoxyisobutylisonitrile (^{99m}Tc-MIBI) is a lipophilic cation isonitrile compound that crosses the cell membrane due to the negative transmembrane potential and accumulates in mitochondria [56, 57]. Because of their higher metabolic activity, tumor cells show large differences in mitochondrial membrane potential and high numbers of mitochondria, making ^{99m}Tc-MIBI an attractive agent in tumor imaging (see Fig. 1). Indeed, studies have demonstrated that good responders of anti-tumor treatment display more MIBI accumulation as compared to poor responders in various tumor types, including small cell and non-small cell lung cancer [58–64], breast cancer [65], malignant lymphoma [66], osteosarcoma [67], and nasopharyngeal carcinoma [68]. One explanation for this phenomenon could be the overexpression of the multidrug resistance gene (MDR1), which encodes P-glycoprotein (Pgp), a transmembrane protein that acts as an efflux pump to a wide range of cytotoxic drugs and ^{99m}Tc-MIBI [69–75], in chemotherapy resistant tumors. Another possibility is the inhibition of mitochondrial membrane permeability as a result of the overexpression of anti-apoptotic proteins such as Bcl-2 [76, 77]. More recently, studies have established a correlation between ^{99m}Tc-MIBI tumor cell uptake and apoptosis after irradiation or chemotherapy [78, 79]. In an unpublished study, Del Vecchio *et al*. [76] demonstrated that the overexpression of Bcl-2 which prevented ^{99m}Tc-MIBI uptake in untreated breast carcinoma could be counteracted by the initiated drug therapy, allowing a transient increase in ^{99m}Tc-MIBI accumulation. The authors speculated that altered expression of proteins participating in the apoptotic process would affect mitochondrial permeability and transmembrane potential, leading to a change in intracellular ^{99m}Tc-MIBI accumulation both prior to and after initiation of therapy. Furthermore, high levels of early ^{99m}Tc-MIBI uptake after treatment [80], could potentially indicate therapeutic efficacy. These results suggest that ^{99m}Tc-MIBI scintigraphy has important clinical implications in providing prognostic information prior to treatment and also in monitoring effectiveness of treatment after initiation of anticancer therapy.

Caspase-3 tracers

Several groups have developed novel PET probes designed to non-invasively image caspase-3 activation, including the small-molecule caspase inhibitor, Isatin, used with different radioisotopes (see Fig. 1). Several of these ^{11}C or ^{18}F Isatins examined *in vivo* [81–87] demonstrated high affinity to caspase-3 and high uptake in the liver in response to cycloheximide or anti-CD95 antibody, confirmed by immunohistology of cell death. Although the radiolabeled Isatins appear to bind specifically to caspase-3, their sensitivity is limited, indicating that further optimization is required for clinical application of these tracers.

Coppola *et al*. [88] generated stable cell lines transfected with a hybrid luciferase reported construct, which is activated by caspase-3 cleavage. Using this system, the apoptotic response of D54 glioma xenograft tumors to temozolomide and radiation was monitored by detecting bioluminescence emission. Apoptosis was detected within 6 h after 4 Gy of radiation in mice receiving the combination treatment. Although this method appeared to be very sensitive and quantitative, the experience seemed to be limited to several animal models [85, 89]. No published patient data are available thus far. In addition, it has recently been found that caspase-3 activation is not unique to apoptosis [90, 91] and is involved in other physiological processes such as platelet aggregation and secretion of enzymes from pancreatic acinar cells.

CONCLUDING REMARKS

This review focuses on *in vivo* apoptosis imaging as a clinical biomarker of response to treatment. In evaluating radiotracers for apoptosis imaging, there are a number of issues to consider. First, the tumor is heterogeneous and consists of a mixture of different cell types and no tracer discussed displays sufficient specificity to identify subpopulations of tumor cells undergoing primary apoptosis. In fact, different types of cell death can be induced by anticancer therapy and exist within the same tumor, including "secondary" apoptosis due to incomplete DNA damage repair (after "mitotic death" or "mitotic catastrophe" or "reproductive cell death" [92, 93]). Second, because response to therapy is tumor type-dependent, the optimal timing of *in vivo* imaging remains to be defined. Though ^{99m}Tc-annexin V scintigraphy has emerged as an attractive

candidate due to its predictive potential in treatment effectiveness in various tumor types, it is not an exclusive marker for this type of cell death, as cellular necrosis accommodates binding of annexin V to exposed membrane PS as well. Therefore, further studies are needed to evaluate the applicability of this and other potential apoptotic markers in daily clinical practice.

REFERENCES

1. **Leist M, Jaattela M.** Four deaths and a funeral: from caspases to alternative mechanisms. Nat Rev Mol Cell Biol 2001; **2**: 589–98.

2. **Dubray B, Breton C, Delic J, *et al.*** *In vitro* radiation-induced apoptosis and early response to low-dose radiotherapy in non-Hodgkin's lymphomas. Radiother Oncol 1998; **46**: 185–91.

3. **Jansen B, Wacheck V, Heere-Ress E, *et al.*** Chemosensitization of malignant melanoma by BCL2 antisense therapy. Lancet 2000; **356**: 1728–33.

4. **Symmans WF, Volm MD, Shapiro RL, *et al.*** Paclitaxel-induced apoptosis and mitotic arrest assessed by serial fine-needle aspiration: implications for early prediction of breast cancer response to neoadjuvant treatment. Clin Cancer Res 2000; **6**: 4610–7.

5. **Meyn RE, Stephens LC, Hunter NR, *et al.*** Apoptosis in murine tumors treated with chemotherapy agents. Anticancer Drugs 1995; **6**: 443–50.

6. **Ellis PA, Smith IE, McCarthy K, *et al.*** Preoperative chemotherapy induces apoptosis in early breast cancer. Lancet 1997; **349**: 849.

7. **Orrenius S.** Apoptosis: molecular mechanisms and implications for human disease. J Intern Med 1995; **237**: 529–36.

8. **Fadeel B, Orrenius S, Zhivotovsky B.** Apoptosis in human disease: a new skin for the old ceremony. Biochem Biophys Res Commun 1999; **266**: 699–717.

9. **Reed JC.** Apoptosis-based therapies. Nat Rev Drug Discov 2002; **1**: 111–21.

10. **Mullauer L, Gruber P, Sebinger D, *et al.*** Mutations in apoptosis genes: a pathogenetic factor for human disease. Mutat Res 2001; **488**: 211–31.

11. **Wu J.** Apoptosis and angiogenesis: two promising tumor markers in breast cancer. Anticancer Res 1996; **16**: 2233–9.

12. **Olson M, Kornbluth S.** Mitochondria in apoptosis and human disease. Curr Mol Med 2001; **1**: 91–122.

13. **Ameisen JC.** On the origin, evolution, and nature of programmed cell death: a timeline of four billion years. Cell Death Differ 2002; **9**: 367–93.

14. **Meyn RE, Milas L, Ang KK.** The role of apoptosis in radiation oncology. Int J Radiat Biol 2009; **85**: 107–15.

15. **Wang X.** The expanding role of mitochondria in apoptosis. Genes Dev 2001; **15**: 2922–33.

16. **Datta R, Kojima H, Yoshida K, *et al.*** Caspase-3-mediated cleavage of protein kinase C theta in induction of apoptosis. J Biol Chem 1997; **272**: 20317–20.

17. **Tepper AD, de Vries E, van Blitterswijk WJ, *et al.*** Ordering of ceramide formation, caspase activation, and mitochondrial changes during CD95- and DNA damage-induced apoptosis. J Clin Invest 1999; **103**: 971–8.

18. **Hannun YA.** Apoptosis and the dilemma of cancer chemotherapy. Blood 1997; **89**: 1845–53.

19. **Sentman CL, Shutter JR, Hockenbery D, *et al.*** bcl-2 inhibits multiple forms of apoptosis but not negative selection in thymocytes. Cell 1991; **67**: 879–88.

20. **Strasser A, Harris AW, Jacks T, *et al.*** DNA damage can induce apoptosis in proliferating lymphoid cells via p53-independent mechanisms inhibitable by Bcl-2. Cell 1994; **79**: 329–39.

21. **Kharbanda S, Ren R, Pandey P, *et al.*** Activation of the c-Abl tyrosine kinase in the stress response to DNA-damaging agents. Nature 1995; **376**: 785–8.

22. **Miyashita T, Krajewski S, Krajewska M, *et al.*** Tumor suppressor p53 is a regulator of bcl-2 and bax gene expression *in vitro* and *in vivo*. Oncogene 1994; **9**: 1799–805.

23. **Miyashita T, Reed JC.** Tumor suppressor p53 is a direct transcriptional activator of the human bax gene. Cell 1995; **80**: 293–9.

24. **Fei P, Bernhard EJ, El-Deiry WS.** Tissue-specific induction of p53 targets *in vivo*. Cancer Res 2002; **62**: 7316–27.

25. **Mihara M, Erster S, Zaika A, *et al.*** p53 has a direct apoptogenic role at the mitochondria. Mol Cell 2003; **11**: 577–90.

26. **Friesen C, Herr I, Krammer PH, *et al.*** Involvement of the CD95 (APO-1/FAS) receptor/ligand system in drug-induced apoptosis in leukemia cells. Nat Med 1996; **2**: 574–7.

27. **Müller M, Strand S, Hug H, *et al.*** Drug-induced apoptosis in hepatoma cells is mediated by the CD95 (APO-1/Fas) receptor/ligand system and involves activation of wild-type p53. J Clin Invest 1997; **99**: 403–13.

28. **Verbrugge I, de Vries E, Tait WG, *et al.*** Ionizing radiation modulates the TRAIL death-inducing signaling complex, allowing bypass of the mitochondrial apoptosis pathway. Oncogene 2008; **27**: 574–84.

29. **Smith C, Gibson DF, Tait JF.** Transmembrane voltage regulates binding of annexin V and lactadherin to cells with exposed phosphatidylserine. BMC Biochem 2009; **10**: 5.

30. **Lahorte CM, Vanderheyden JL, Steinmetz N, *et al.*** Apoptosis-detecting radioligands: current state of the art and future perspectives. Eur J Nucl Med Mol Imaging 2004; **31**: 887–919.

31. **Stratton JR, Dewhurst TA, Kasina S, *et al.*** Selective uptake of radiolabeled annexin V on acute porcine left atrial thrombi. Circulation 1995; **92**: 3113–21.

32. **Tait JF.** Imaging of apoptosis. J Nucl Med 2008; **49**: 1573–6.

33. **Blankenberg FG, Katsikis PD, Tait JF, *et al.*** Imaging of apoptosis (programmed cell death) with ^{99m}Tc annexin V. J Nucl Med 1999; **40**: 184–91.

34. **Blankenberg FG.** Monitoring of treatment-induced apoptosis in oncology with PET and SPECT. Curr Pharm Des 2008; **14**: 2974–82.

35. **Kemerink GJ, Boersma HH, Thimister PW, *et al.*** Biodistribution and dosimetry of 99mTc-BTAP-annexin-V in humans. Eur J Nucl Med 2001; **28**: 1373–8.

36. **Kemerink GJ, Liu X, Kieffer D, *et al.*** Safety, biodistribution, and dosimetry of ^{99m}Tc-HYNIC-annexin V, a novel human recombinant annexin V for human application. J Nucl Med 2003; **44**: 947–52.

37. **Hofstra L, Liem IH, Dumont EA, *et al.*** Visualisation of cell death *in vivo* in patients with acute myocardial infarction. Lancet 2000; **356**: 209–12.

38. **Penn DL, Kim C, Zhang K, *et al.*** Apoptotic abscess imaging with ^{99m}Tc-HYNIC-rh-Annexin-V. Nucl Med Biol 2010; **37**: 29–34.

39. **Blankenberg FG, Katsikis PD, Tait JF, *et al.*** *In vivo* detection and imaging of phosphatidylserine expression during programmed cell death. Proc Natl Acad Sci USA 1998; **95**: 6349–54.

40. **Beekman CA, Buckle T, van Leeuwen AC, *et al.*** Questioning the value of (99m)Tc-HYNIC-annexin V based response monitoring after docetaxel treatment in a mouse model for hereditary breast cancer. Appl Radiat Isot 2011; **69**: 656–62.

41. **Belhocine T, Steinmetz N, Hustinx R, *et al.*** Increased uptake of the apoptosis-imaging agent (99m)Tc recombinant human Annexin V in human tumors after one course of chemotherapy as a predictor of tumor response and patient prognosis. Clin Cancer Res. 2002; **8**: 2766–74.

42. **Haas RL, de Jong D, Valdés Olmos RA, *et al.*** *In vivo* imaging of radiation-induced apoptosis in follicular lymphoma patients. Int J Radiat Oncol Biol Phys 2004; **59**: 782–7.

43. **Kartachova M, Haas RL, Olmos RA, *et al.*** *In vivo* imaging of apoptosis by ^{99m}Tc-Annexin V scintigraphy: visual analysis in relation to treatment response. Radiother Oncol 2004; **72**: 333–9.

44. **Kartachova M, van Zandwijk N, Burgers S, *et al.*** Prognostic significance of ^{99m}Tc Hynic-rh-annexin V scintigraphy during platinum-based chemotherapy in advanced lung cancer. J Clin Oncol 2007; **25**: 2534–9.

45. **Kartachova MS, Valdes Olmos RA, Haas RL, *et al.*** ^{99m}Tc-HYNIC-rh-annexin-V scintigraphy: visual and quantitative evaluation of early treatment-induced apoptosis to predict treatment outcome. Nucl Med Commun 2008; **29**: 39–44.

46. **Hoebers FJ, Kartachova M, de Bois J, *et al.*** ^{99m}Tc Hynic-rh-Annexin V scintigraphy for *in vivo* imaging of apoptosis in patients with head and neck cancer treated with chemoradiotherapy. Eur J Nucl Med Mol Imaging 2008; **35**: 509–18.

47. **van de Wiele C, Lahorte C, Vermeersch H, *et al.*** Quantitative tumor apoptosis imaging using technetium-99m-HYNIC annexin V single photon emission computed tomography. J Clin Oncol 2003; **21**: 3483–7.

48. **Verheij M, van Blitterswijk WJ, Bartelink H.** Radiation-induced apoptosis — the ceramide-SAPK signaling pathway and clinical aspects. Acta Oncol 1998; **37**: 575–81.

49. **Loose D, Vermeersch H, De Vos F, *et al.*** Prognostic value of ^{99m}Tc-HYNIC annexin-V imaging in squamous cell carcinoma of the head and neck. Eur J Nucl Med Mol Imaging 2008; **35**: 47–52.

50. **Blankenberg FG.** *In vivo* detection of apoptosis. J Nucl Med 2008; **49** (Suppl 2): 81S–95S.

51. **Cohen A, Shirvan A, Levin G, *et al.*** From the Gla domain to a novel small-molecule detector of apoptosis. Cell Res 2009; **19**: 625–37.

52. **Cohen A, Ziv I, Aloya T, *et al.*** Monitoring of chemotherapy-induced cell death in melanoma tumors by N,N'-Didansyl-L-cystine. Technol Cancer Res Treat 2007; **6**: 221–34.

53. **Aloya R, Shirvan A, Grimberg H, *et al.*** Molecular imaging of cell death *in vivo* by a novel small molecule probe. Apoptosis 2006; **11**: 2089–101.

54. **Grimberg H, Levin G, Shirvan A, *et al.*** Monitoring of tumor response to chemotherapy *in vivo* by a novel small-molecule detector of apoptosis. Apoptosis 2009; **14**: 257–67.

55. **Allen AM, Ben-Ami M, Reshef A, *et al.*** Assessment of response of brain metastases to radiotherapy by PET imaging of apoptosis with (18)F-ML-10. Eur J Nucl Med Mol Imaging 2012; **39**: 1400–8.

56. **Chiu ML, Kronauge JF, Piwnica-Worms D.** Effect of mitochondrial and plasma membrane potentials on accumulation of hexakis (2-methoxyisobutylisonitrile) technetium(I) in cultured mouse fibroblasts. J Nucl Med 1990; **31**: 1646–53.

57. **Wackers FJ, Berman DS, Maddahi J, *et al.*** Technetium-99m hexakis 2-methoxyisobutyl isonitrile: human biodistribution, dosimetry, safety, and preliminary comparison to thallium-201 for myocardial perfusion imaging. J Nucl Med 1989; **30**: 301–11.

58. **Bom HS, Kim YC, Song HC, *et al.*** Technetium-99m-MIBI uptake in small cell lung cancer. J Nucl Med 1998; **39**: 91–4.

59. **Ceriani L, Giovanella L, Bandera M, *et al.*** Semiquantitative assessment of 99Tcm-sestamibi uptake in lung cancer: relationship with clinical response to chemotherapy. Nucl Med Commun 1997; **18**: 1087–97.

60. **Kao CH, ChangLai SP, Chieng PU, *et al.*** Technetium-99m methoxyisobutylisonitrile chest imaging of small cell lung carcinoma: relation to patient prognosis and chemotherapy response — a preliminary report. Cancer 1998; **83**: 64–8.

61. **Kao CH, Hsieh JF, Tsai SC, *et al.*** Quickly predicting chemotherapy response to paclitaxel-based therapy in non-small cell lung cancer by early technetium-99m methoxyisobutylisonitrile chest single-photon-emission computed tomography. Clin Cancer Res 2000; **6**: 820–4.

62. **Nishiyama Y, Yamamoto Y, Satoh K, *et al.*** Comparative study of Tc-99m MIBI and TI-201 SPECT in predicting chemotherapeutic response in non-small-cell lung cancer. Clin Nucl Med 2000; **25**: 364–9.

63. **Yamamoto Y, Nishiyama Y, Satoh K, *et al.*** Comparative evaluation of Tc-99m MIBI and Tl-201 chloride SPECT in non-small-cell lung cancer mediastinal lymph node metastases. Clin Nucl Med 2000; **25**: 29–32.

64. **Yang TJ, Aukema TS, van Tinteren H, *et al.*** Predicting early chemotherapy response with technetium-99m methoxyisobutylisonitrile SPECT/CT in advanced non-small cell lung cancer. Mol Imaging Biol 2009; **12**: 174–80.

65. **Moretti JL, Azaloux H, Boisseron D, *et al.*** Primary breast cancer imaging with technetium-99m sestamibi and its relation with P-glycoprotein overexpression. Eur J Nucl Med 1996; **23**: 980–6.

66. **Dimitrakopoulou-Strauss A, Strauss LG, Goldschmidt H, *et al.*** Evaluation of tumour metabolism and multidrug resistance in patients with treated malignant lymphomas. Eur J Nucl Med 1995; **22**: 434–42.

67. **Burak Z, Moretti JL, Ersoy O, *et al.*** 99mTc-MIBI imaging as a predictor of therapy response in osteosarcoma compared with multidrug resistance-associated protein and P-glycoprotein expression. J Nucl Med 2003; **44**: 1394–401.

68. **Wang XS, Zhang YJ, Liu XL, *et al.*** The role of technetium-99m methoxyisobutyl isonitrile scintigraphy in predicting the therapeutic effect of chemotherapy against nasopharyngeal carcinoma. Cancer 2010 [Epub ahead of print].

69. **Bellamy WT.** P-glycoproteins and multidrug resistance. Annu Rev Pharmacol Toxicol 1996; **36**: 161–83.

70. **Gottesman MM, Pastan I.** Biochemistry of multidrug resistance mediated by the multidrug transporter. Annu Rev Biochem 1993; **62**: 385–427.

71. **Muzzammil T, Moore MJ, Hedley D, *et al.*** Comparison of (99m)Tc-sestamibi and doxorubicin to monitor inhibition of P-glycoprotein function. Br J Cancer 2001; **84**: 367–73.

72. **Germann UA.** P-glycoprotein — a mediator of multidrug resistance in tumour cells. Eur J Cancer 1996; **32A**: 927–44.

73. **Muzzammil T, Ballinger JR, Moore MJ.** 99Tcm-sestamibi imaging of inhibition of the multidrug resistance transporter in a mouse xenograft model of human breast cancer. Nucl Med Commun 1999; **20**: 115–22.

74. **Del Vecchio S, Ciarmiello A, Salvatore M.** Clinical imaging of multidrug resistance in cancer. Q J Nucl Med 1999; **43**: 125–31.

75. **Kao A, Shiun SC, Hsu NY, *et al.*** Technetium-99m methoxyisobutylisonitrile chest imaging for small-cell lung cancer. Relationship to chemotherapy response (six courses of combination of cisplatin and etoposide) and p-glycoprotein or multidrug resistance related protein expression. Ann Oncol 2001; **12**: 1561–6.

76. **Del Vecchio S, Salvatore M.** ^{99m}Tc-MIBI in the evaluation of breast cancer biology. Eur J Nucl Med Mol Imaging 2004; **31** (Suppl 1): S88–96.

77. **Del Vecchio S, Zannetti A, Aloj L, *et al.*** Inhibition of early 99mTc-MIBI uptake by Bcl-2 anti-apoptotic protein overexpression in untreated breast carcinoma. Eur J Nucl Med Mol Imaging 2003; **30**: 879–87.

78. **Zhu X, Wu H, Xia J, *et al.*** The relationship between (99m)Tc-MIBI uptakes and tumor cell death/proliferation state under irradiation. Cancer Lett 2002; **182**: 217–22.

79. **Vergote J, Di Benedetto M, Moretti JL, *et al.*** Could 99mTc-MIBI be used to visualize the apoptotic MCF7 human breast cancer cells? Cell Mol Biol 2001; **47**: 467–71.

80. **Ciarmiello A, Del Vecchio S, Silvestro P, *et al.*** Tumor clearance of technetium 99m-sestamibi as a predictor of response to neoadjuvant chemotherapy for locally advanced breast cancer. J Clin Oncol 1998; **16**: 1677–83.

81. **Chen DL, Zhou D, Chu W, *et al.*** Comparison of radiolabeled isatin analogs for imaging apoptosis with positron emission tomography. Nucl Med Biol 2009; **36**: 651–78.

82. **Nguyen QD, Smith G, Glaser M, *et al.*** Positron emission tomography imaging of drug-induced tumor apoptosis with a caspase-3/7 specific[18F]-labeled isatin sulfonamide. Proc Natl Acad Sci USA 2009; **106**: 16375–80.

83. **Podichetty AK, Wagner S, Schroer S, *et al.*** Fluorinated isatin derivatives. Part 2. New N-substituted 5-pyrrolidinylsulfonyl isatins as potential tools for molecular imaging of caspases in apoptosis. J Med Chem 2009; **52**: 3484–95.

84. **Zhou D, Chu W, Chen DL, *et al.*** [18F]- and [11C]-labeled N-benzyl-isatin sulfonamide analogues as PET tracers for apoptosis: synthesis, radiolabeling mechanism, and *in vivo* imaging study of apoptosis in Fas-treated mice using [11C] WC-98. Org Biomol Chem 2009; **7**: 1337–48.

85. **Zhou D, Chu W, Rothfuss J, *et al.*** Synthesis, radiolabeling, and *in vivo* evaluation of an 18F-labeled isatin analog for imaging caspase-3 activation in apoptosis. Bioorg Med Chem Lett 2006; **16**: 5041–6.

86. **Kopka K, Faust A, Keul P, *et al.*** 5-pyrrolidinylsulfonyl isatins as a potential tool for the molecular imaging of caspases in apoptosis. J Med Chem 2006; **49**: 6704–15.

87. **Chen DL, Zhou D, Chu W, *et al.*** Radiolabeled isatin binding to caspase-3 activation induced by anti-Fas antibody. Nucl Med Biol 2012; **39**: 137–44.

88. **Coppola JM, Ross BD, Rehemtulla A.** Noninvasive imaging of apoptosis and its application in cancer therapeutics. Clin Cancer Res 2008; **14**: 2492–501.

89. **Faust A, Wagner S, Law MP, *et al.*** The nonpeptidyl caspase binding radioligand (S)-1-(4-(2-[18F]Fluoroethoxy)-benzyl)-5-[1-(2-methoxymethylpyrrolidinyl)sulfonyl]isatin ([18F]CbR) as potential positron emission tomography-compatible apoptosis imaging agent. Q J Nucl Med Mol Imaging 2007; **51**: 67–73.

90. **Rosado JA, Lopez JJ, Gomez-Arteta E, *et al.*** Early caspase-3 activation independent of apoptosis is required for cellular function. J Cell Physiol 2006; **209**: 142–52.

91. **Spires-Jones TL, de Calignon A, Matsui T, *et al.*** *In vivo* imaging reveals dissociation between caspase activation and acute neuronal death in tangle-bearing neurons. J Neurosci 2008; **28**: 862–7.

92. **Endlich B, Radford IR, Forrester HB, *et al.*** Computerized video time-lapse microscopy studies of ionizing radiation-induced rapid-interphase and mitosis-related apoptosis in lymphoid cells. Radiation Research 2000; **153**: 36–48.

93. **Verheij M.** Clinical biomarkers and imaging for radiotherapy-induced cell death. Cancer Metastasis Rev 2008; **27**: 471–80.

94. **Haimovitz-Friedman A, Yang TI, Thin TH, Verheij M.** Imaging radiotherapy-induced apoptosis. Radiat Res 2012; **177**: 467–82.